

## Supplemental Material

### Supplementary Fig. 1. EETs stimulate primary tumor growth.

**a)** Schematic presentation of genetic and pharmacological tools used to manipulate endogenous EET levels.

**b)** Endothelial cells isolated from Tie2-CYP2J2-Tr and Tie2-CYP2C8-Tr mice secrete significantly more 14,15-EET than cells isolated from WT mice (left panel). Endothelial cells isolated from Tie2-sEH-Tr mice secrete significantly less 14,15-EET than cells isolated from WT mice (right panel). Values are in pg per million cells. n=3-4 per group; \* $P=0.021$  vs. WT; \*\* $P=0.016$  vs. WT; \*\*\* $P=0.003$  vs. WT.

**c)** Growth of T241 fibrosarcoma, B16F10 melanoma and LLC primary tumors in Tie2-CYP2C8-Tr, Tie2-CYP2J2-Tr, and WT mice. Blue insets show representative tumors on day 22 (T241 fibrosarcoma) or day 31 (B16F10 melanoma) post-injection. Scale bar, 1cm. n=5-13 mice/group; \* $P=0.049$  vs. WT; \*\* $P=0.032$  vs. WT; \*\*\* $P=0.011$  vs. WT.

**d)** Increase in plasma 14,15-EET and 11,12-EET in sEH-null mice (day 22 post-T241 fibrosarcoma injection) and plasma 14,15-EET in Tie2-CYP2C8-Tr mice (day 16 post-LLC injection) relative to WT mice as measured by LC/MS/MS. n=5 mice/group (sEH-null mice) and n=6-8 mice/group (Tie2-CYP2C8-Tr and WT mice); \* $P=0.011$  vs. WT; \*\* $P=0.016$  vs. WT; \*\*\* $P=0.044$  vs. WT.

**e)** EET levels are not changed in the tumor tissue (T241 fibrosarcoma) on day 22 post-injection in Tie2-CYP2C8-Tr and sEH-null mice relative to WT mice as measured by LC/MS/MS. n=5-8 mice/group.

**f)** 14,15-EET (15  $\mu\text{g}/\text{kg}/\text{day}$ ) stimulates orthotopic human prostate cancer growth (PC3M-LN4). n=5-6 mice/group; \* $P=0.021$  vs. vehicle control.

**g)** 14,15-EET levels are not changed in tumors isolated from TRAMP mice relative to normal mouse prostates from age-matched control mice as measured by LC/MS/MS. n=8-10

mice/group.

**h)** Increase in plasma epoxygenase activity (sum of 14,15-EET + 14,15-DHET) in TRAMP mice relative to age-matched control mice as measured by LC/MS/MS. Plasma from TRAMP mice show increased 14,15-DHET but not 14,15-EET relative to control mice. n=7-9 mice/group. \* $P < 0.05$  vs. control.

**i)** Vessel density, as defined by the number of CD31-positive blood vessels, is increased in B16F10 melanoma in Tie2-CYP2C8-Tr, Tie2-CYP2J2-Tr, and sEH-null mice relative to WT mice on day 22 post-tumor implantation. The left panel show photomicrographs (Scale bar, 20  $\mu\text{m}$ ) and the right panel shows number of vessels per high power field (HPF). n=5 mice per group; \* $P < 0.001$  vs. WT.

**j)** Tumor angiogenesis as quantified by flow cytometry analysis of CD31+/CD45- endothelial cells (ECs) in LLC on day 22 post-injection. Tumor ECs are increased 3-fold in Tie2-CYP2J2-Tr mice compared to WT mice. n=5 tumors/group; \* $P = 0.029$  vs. WT.

**k)** Vessel density, as defined by the number of CD31-positive blood vessels, is increased in 14,15-EET treated TRAMP and PC3M-LN4 tumors relative to vehicle-treated control tumors. The left and middle panel show photomicrographs (Scale bar, 100  $\mu\text{m}$ ) and the right panel shows number of vessels per high power field (HPF). n=5 mice per group; \* $P < 0.05$  vs. control. Brown (DAB staining of CD31-positive vessels).

**l)** Vessel density is decreased in T241 fibrosarcoma in Tie2-sEH-Tr mice relative to WT mice on day 28 post-tumor implantation; The left and middle panel show photomicrographs (Scale bar, 100  $\mu\text{m}$ ) and the right panel shows number of vessels per high power field (HPF). n=4-6 mice per group; \* $P < 0.05$  vs. control. Brown (DAB staining of CD31-positive vessels).

**m)** Corneal tumor angiogenesis induced by LLC is increased in Tie2-CYP2C8-Tr and sEH-null mice on day 7 and 10 post-injection, respectively, relative to WT mice where it was increased only by day 13. Photos are representative of n=5 eyes/group.

**n)** Corneal tumor angiogenesis induced by LLC-GFP is increased in mice treated systemically with 14,15-EET on day 19. n=5 eyes/group. \* $P=0.024$  vs. Control.

**o)** Corneal tumor angiogenesis induced by B16F10 melanoma is increased in mice treated systemically with 14,15-EET on day 21. Photos on day 21 are representative of n=5-6 eyes/group (left upper panel). Flow cytometry of B16F10 melanoma tumors show a 21% increase in CD31-positive endothelial cells in 14,15-EET treated mice in comparison to vehicle-treated mice (right upper panel). Raw flow data is shown in lower panel. n=4-5 corneas/group; \* $P=0.038$  vs. vehicle control.

**p)** Depletion of macrophages with clodronate liposomes has no effect on LLC tumor growth in 14,15-EET treated mice (lower left panel) and Tie2-CYP2C8 Tr mice (lower right panel). Flow cytometry demonstrates significant depletion of macrophages (CD45+, F4/80+) in mice treated with clodronate liposomes (upper left panel). Raw flow data of one sample pair is shown in upper right panel. n=5-6 mice per group. MQ= macrophage depleted. \* $P<0.05$  vs. vehicle control (empty liposome).

**Supplementary Fig. 2. EETs trigger spontaneous multi-organ metastasis.**

**a)** Tie2-CYP2C8-Tr and sEH-null mice exhibit liver and kidney metastasis (arrows) 10 days post LLC resection whereas WT mice do not. Representative photos are shown. Scale bar, 1cm.

**b)** Spontaneous LLC metastasis to lungs is decreased in Tie2-sEH-Tr vs. WT mice on day 17 post-LLC resection. Representative photos are shown. Scale bar, 1cm.

**c)** Tie2-CYP2J2-Tr mice have increased LLC metastasis to the lung on day 22 post-LLC injection without resection. The left panel shows number of surface metastases and lung weight. The middle panel shows representative photos. N=6 mice per group; Scale bar, 1cm. Spontaneous LLC axillary lymph node metastasis occurs in Tie2-CYP2J2-Tr but not in WT mice by day 22 post-injection (right panel). Blue inset shows representative right axillary lymph node metastases 22 days post-injection of LLC from four Tie2-CYP2J2-Tr mice (arrow indicates axillary lymph node cut in half). n=6 mice/group; \* $P=0.028$  vs. WT; \*\* $P=0.024$  vs. WT \*\*\* $P=0.002$  vs. WT. Scale bar, 1 cm.

**d)** Representative H&E stained section of axillary lymph node metastasis 22 days post-injection of LLC in Tie2-CYP2J2-Tr mice shows metastatic LLC tumor cells (arrows). Scale bar, 20  $\mu\text{m}$ .

**e)** B16F10 melanoma metastasis to lung is increased in Tie2-CYP2C8-Tr mice relative to WT 18 days after tail vein injection. The left panel shows lung weight and number of surface metastases. Blue insets show representative lung and liver metastasis in Tie2-CYP2C8-Tr mice (right panel). WT mice do not develop liver metastasis. n=6 mice/group; \* $P<0.05$  vs. WT. Scale bar, 1 cm.

**f)** Upper panel shows representative axillary lymph node metastasis 17 days post-B16F10 resection in WT, Tie2-CYP2C8-Tr and sEH-null mice; Scale bar, 1 cm. H&E stained sections of axillary lymph nodes confirm B16F10 tumor cell metastasis (middle panel); Scale bar, 20  $\mu\text{m}$ .

Lower panel demonstrates more than a 2-fold increase in lymph node metastasis in Tie2-CYP2C8-Tr and sEH-null vs. WT mice. n=6 mice/group; \* $P < 0.001$  vs. WT.

**g)** Systemic administration of 14,15-EET (15  $\mu\text{g}/\text{kg}/\text{day}$ ) via mini-osmotic pump increases spontaneous LLC distant axillary lymph node metastasis 12 days post LLC resection. White circle indicates representative metastatic lymph node metastasis. Scale bar 1cm.

**h)** Systemic administration of 14,15-EET (15  $\mu\text{g}/\text{kg}/\text{day}$ ) via minipump increases lung, liver, and kidney metastasis 19 days post B16F10-GFP intravenous injection. Arrows point to representative lung, liver, and kidney metastasis in 14,15-EET treated mice. Scale bar, 1cm.

**Supplementary Fig. 3. Pharmacological manipulation of EET levels controls primary tumor growth and metastasis.**

**a)** Analysis of plasma from LLC-GFP tumor bearing mice treated with the sEH inhibitor *t*AUCB (10 mg/kg/day) reveals an increase in plasma EETs by LC/MS/MS. n=5 mice per group; \* $P < 0.05$  vs. vehicle.

**b)** Analysis of tumor tissue (LLC-GFP tumors) from mice treated with *t*AUCB showed no change in EET levels relative to vehicle-treated mice by LC/MS/MS. n=5 mice per group.

**c)** Negative control (no primary antibody) for immunofluorescent double staining for VEGF and GFP (tumor cells). Green, GFP-stained tumor cells; red, VEGF-containing cells. Scale bar, 20  $\mu\text{m}$ .

**d)** Systemic administration of sEH inhibitors *t*AUCB and TUPS (10 mg/kg/day each) increases lung and liver metastasis. The upper panel shows lung weight and number of surface metastases; lower middle panel shows liver weight. *t*AUCB and TUPS induce liver metastasis in the spontaneous LLC metastasis model after 12 days of treatment post LLC resection. Vehicle-treated mice do not develop liver metastasis. Representative lungs and livers after 12 days of treatment (bottom panel). Scale bar, 1 cm. n=8 mice/group; \* $P = 0.032$  vs. control; \*\* $P = 0.004$  vs. control; \*\*\* $P = 0.042$  vs. control; \*\*\*\* $P = 0.043$  vs. control.

**e)** 14,15-EET promotes spontaneous axillary lymph node metastasis 28 days post B16F10-GFP tumor resection to over 10-20% of body weight (left panel); scale bar, 1cm. GFP-labeled tumor cells in the lymph node are stained green (right panel); scale bar 5 mm. n=5 mice per group.

**f)** 14,15-EET promotes spontaneous axillary lymph node metastasis 25 days post B16F10-GFP tumor resection. GFP-labeled tumor cells in the lymph node are stained green (left panel). Scale bar 500  $\mu\text{m}$ . Low power image of H&E staining (20x) demonstrates a cross-section of skin with an underlying lymph node replaced by metastatic tumor (right panel). High power magnification (400x) shows sheets of pleomorphic variably sized tumor cells comprising greater than 95% of the mass of the lymph node. Scale bar, 50  $\mu\text{m}$ .

**g)** The EET antagonist 14,15-EEZE (0.21 mg/mouse) inhibits lung and lymph node metastases in Tie2-CYP2C8-Tr and sEH-null mice in a spontaneous LLC lung metastasis model n=4-5 mice/group; Blue insets show representative lung metastasis in vehicle-treated and 14,15-EEZE-treated Tie2-CYP2C8-Tr and sEH-null mice on day 17 post LLC resection. Scale bar, 1cm. \* $P < 0.05$  vs vehicle treatment.

**h)** Vessel density is decreased in B16F10-GFP melanoma tumors treated with the EET antagonist 14,15-EEZE (0.21 mg/mouse) for 21 days. Brown (DAB staining of CD31-positive vessels). The left and middle panel show photomicrographs (Scale bar, 100  $\mu\text{m}$ ) and the right panel shows number of vessels per high power field (HPF). n=4-5 mice per group; \* $P < 0.05$  vs. vehicle-treated control.

**Supplementary Fig. 4. Pro-tumorigenic activity of endothelial-derived EETs is mediated by VEGF and loss of TSP1.**

**a)** Tie2-sEH-Tr mice exhibit endothelial-specific staining of sEH in the liver, whereas WT mice do not. Scale bar, 20  $\mu$ m.

**b)** Immunohistochemistry of 14,15-EET treated LLC tumors shows VEGFR2 expression in endothelial cells (middle panel, black arrow), leukocytes (such as a macrophage) (right panel, black arrow), and tumor cells (right panel, red arrows); Scale bar 100  $\mu$ m.

**c)** Immunofluorescent double staining for VEGFR2 and CD45 (pan leukocyte marker) indicates leukocyte expression of VEGFR2 in 14,15-EET treated LLC tumors (left panel). Green, CD45-stained leukocytes; red, VEGFR2-containing cells. Co-localization of red and green fluorescence (yellow) indicates leukocytes expressing VEGFR2 (arrows). Immunofluorescent double staining for VEGFR2 and CD31 (endothelial cell marker) indicates endothelial cell expression of VEGFR2 in 14,15-EET treated LLC tumors (right panel). Green, CD31-stained endothelial cells; red, VEGFR2-containing cells. Co-localization of red and green fluorescence (yellow) indicates tumor endothelial cells expressing VEGFR2 (arrows). Scale bar, 20  $\mu$ m.

**d)** The sEH inhibitor *t*AUCB (10 mg/kg/day) is unable to promote primary LLC growth in mice depleted of VEGF by systemic sFlt. In contrast, primary LLC growth is promoted in *t*AUCB-treated mice receiving control virus.  $n=6$  mice/group;  $*P=0.041$  vs. *t*AUCB + Ad-null. Blue insets show representative photographs of LLC tumors on day 20. Scale bar, 1 cm.

**e)** Stromal TSP1 expression is decreased in three different tumors (LLC, B16F10 melanoma, and T241 fibrosarcoma) in Tie2-CYP2C8-Tr and sEH-null mice compared to WT mice. Scale bar, 100  $\mu$ m. Brown (DAB staining of TSP1).

**f)** 14,15-EET (1  $\mu$ M) specifically decreases TSP1 production in fibroblasts but has no effect on TSP1 production in tumor and endothelial cells *in vitro*; tumor cells (human prostate tumor cells – PC3M-LN4); endothelial cells (human microvascular endothelial cells); and fibroblasts (human).  $*P<0.05$  vs vehicle treatment.

**g)** 14,15-EET (1  $\mu$ M) increases VEGF production by tumor cells and endothelial cells *in vitro* but has no effect on VEGF production in fibroblasts; tumor cells (human prostate tumor cells – PC3M-LN4); endothelial cells (human microvascular endothelial cells); and fibroblasts (human).

\* $P < 0.05$  vs vehicle treatment.

**h)** sEH protein is down-regulated in tumor endothelial cells isolated from TRAMP mice compared to normal murine endothelial cells and to murine prostate tumor cells (TRAMP C1).

**i)** Western blot analysis of sEH, CYP2C, and CYP2J protein in murine tumor cells *in vitro*. Control=mouse liver; LLC=Lewis lung carcinoma, B16F10=B16F10 melanoma, B16BL6=B16BL6 melanoma, T241=T241 fibrosarcoma, EOMA= hemangioendothelioma, MS180=mouse sarcoma 180, BTC=pancreatic beta tumor cell.

**Supplementary Fig. 5. Parabiosis experiments show that EET-stimulated metastasis requires EET-producing endothelium at the metastatic site.**

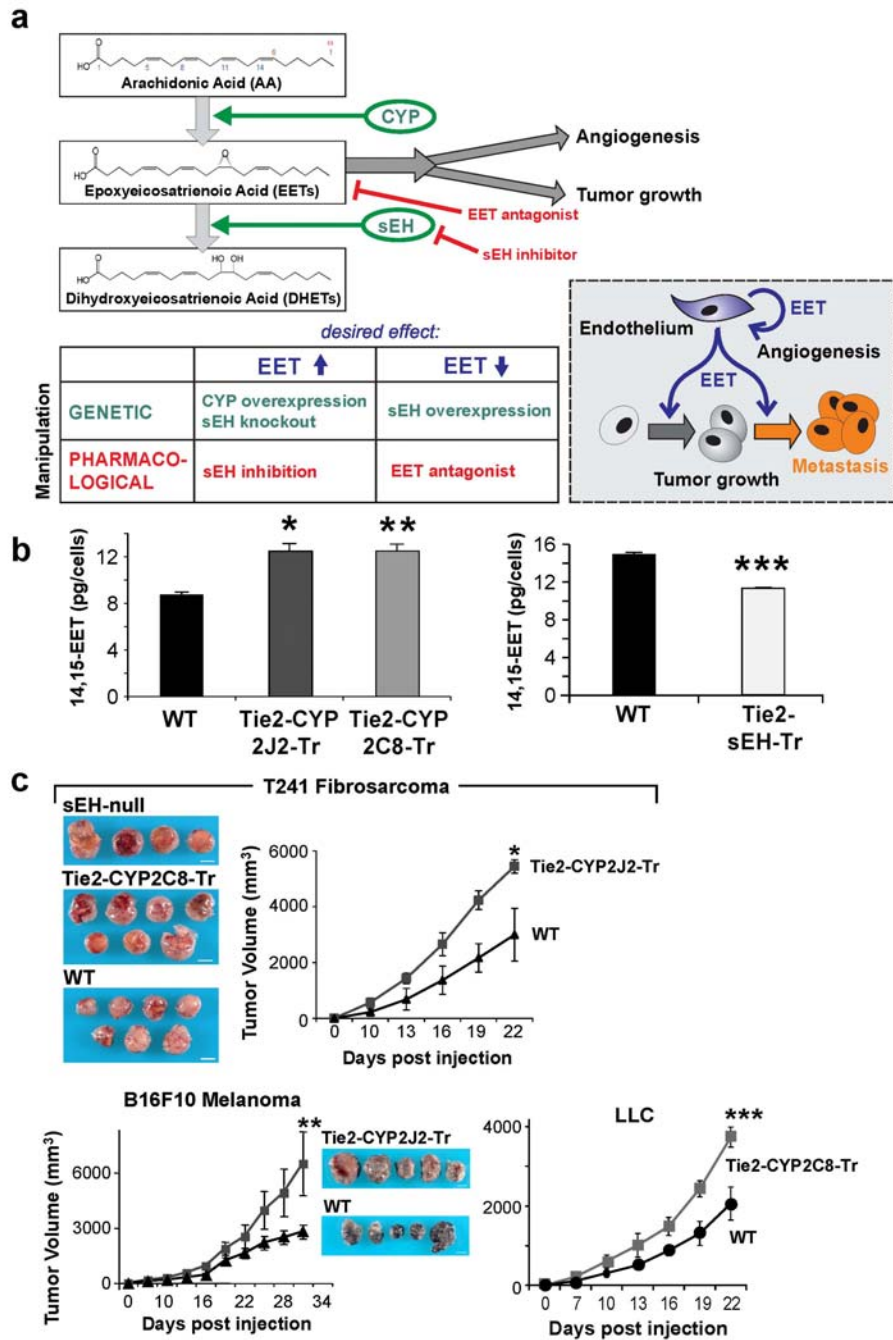
**a)** Cross-circulation between “EET high” and “EET low” mice is demonstrated after one animal in the pair was injected with 100  $\mu$ l of 0.25% Evan’s blue 4 weeks after surgical union. The first organ of the uninjected partner to show blue discoloration 30 minutes after injection is the liver. Scale bar, 1 cm.

**b)** Three hours after injection, Evan’s blue concentrations were equalized in various organs between the injected and uninjected partners. Spectrophotometric analysis of extravasated Evans blue is represented in bar graph. n=5 mice/group.

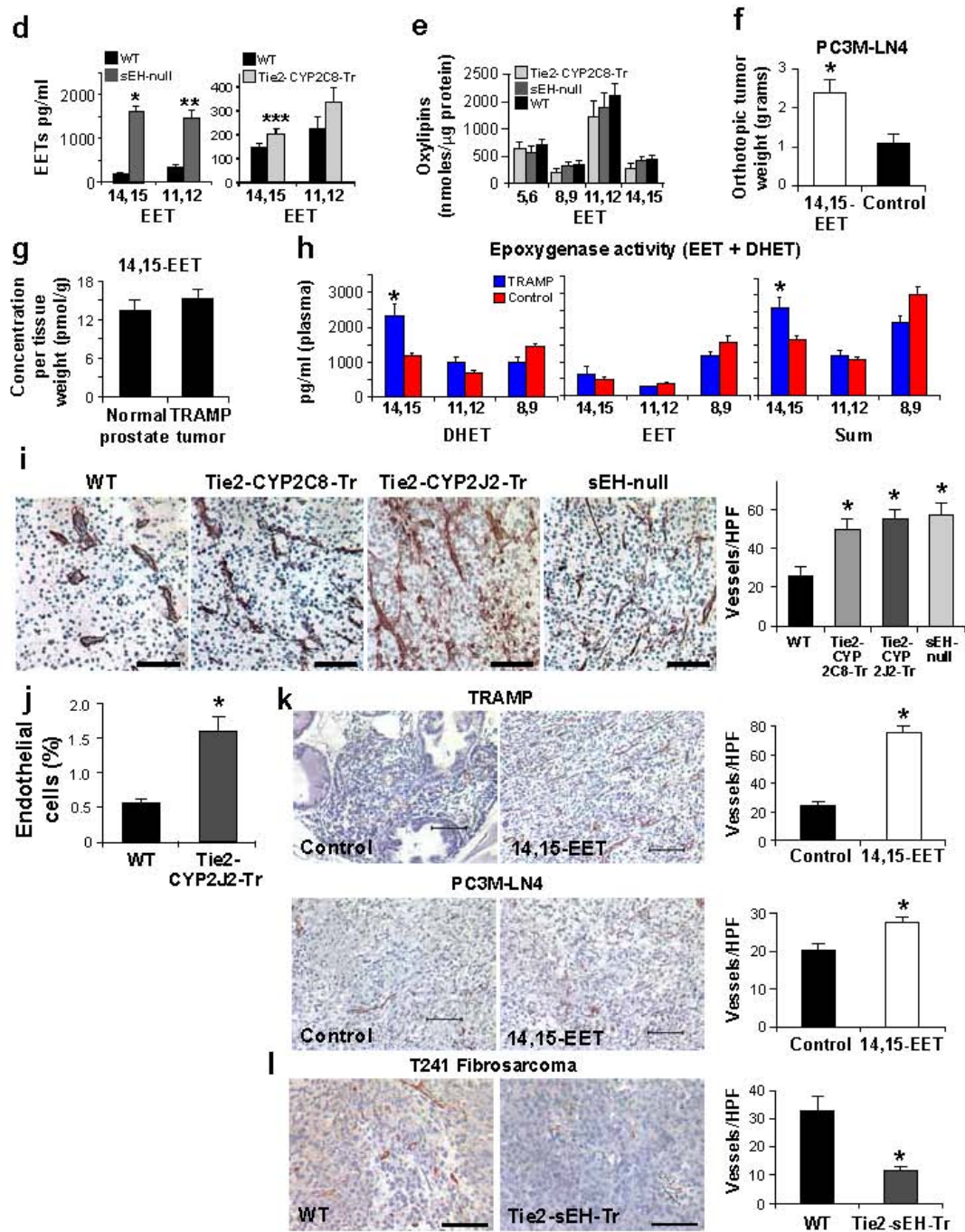
**c)** The genotype of the tumor-bearing mouse (donor) determines growth of the primary tumor, regardless of the genotype of the recipient mouse. However, an EET-producing endothelium is critical at the metastatic site for EET-induced lung, liver and lymph node metastasis. Scale bar, 1 cm. n=4-5 mice/group.

**d)** Adoptive transfer of whole blood from the “low EET” recipient parabiont (Tie2-sEH-Tr), which exhibited no metastasis, into non-parabiosis “high EET” (Tie2-CYP2C8-Tr) mice caused metastatic disease and reduced survival. In contrast, adoptive transfer of whole blood from into WT mice did not cause metastatic disease and survival was 100%. n=5 mice/group.

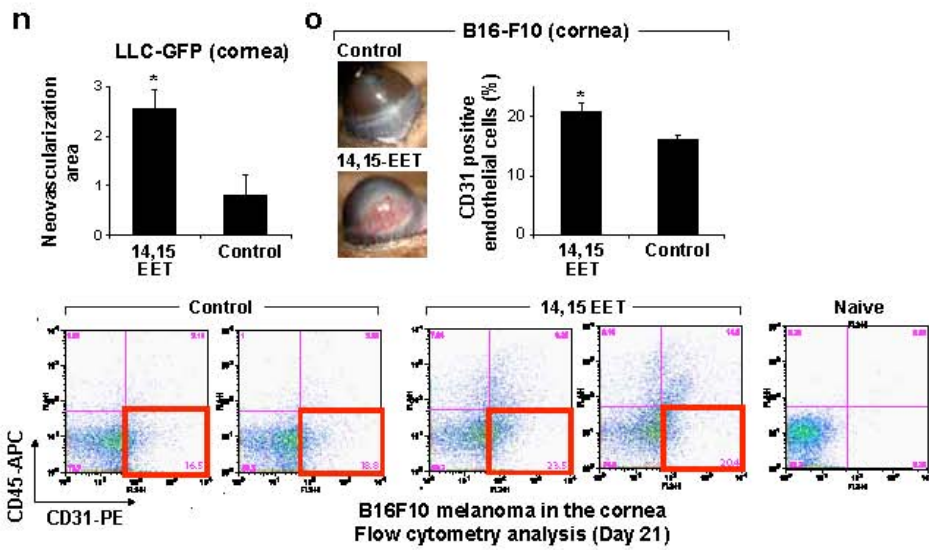
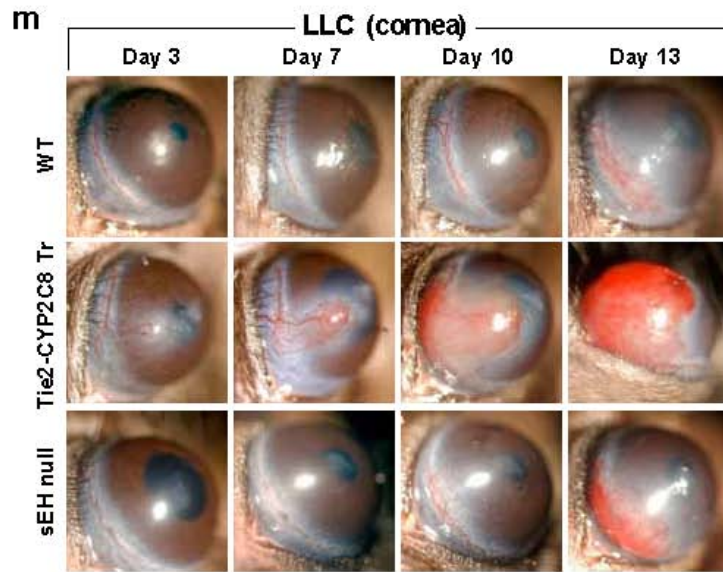
**e)** Immunofluorescence staining of primary LLC tumors of the parabionts show increased tumor endothelial cell proliferation and VEGF production when the genotype of the tumor-bearing mice is Tie2-CYP2C8-Tr (whether joined to another Tie2-CYP2C8-Tr or WT mice); Tie2-CYP2C8-Tr  $\rightarrow$  Tie2-CYP2C8-Tr (tumor bearing); WT  $\rightarrow$  Tie2-CYP2C8-Tr (tumor bearing); WT $\rightarrow$ WT (tumor bearing). MECA-32=green, VEGF=red (left panel); MECA-32=green, Ki67=red (right panel). Scale bar, 20  $\mu$ m.



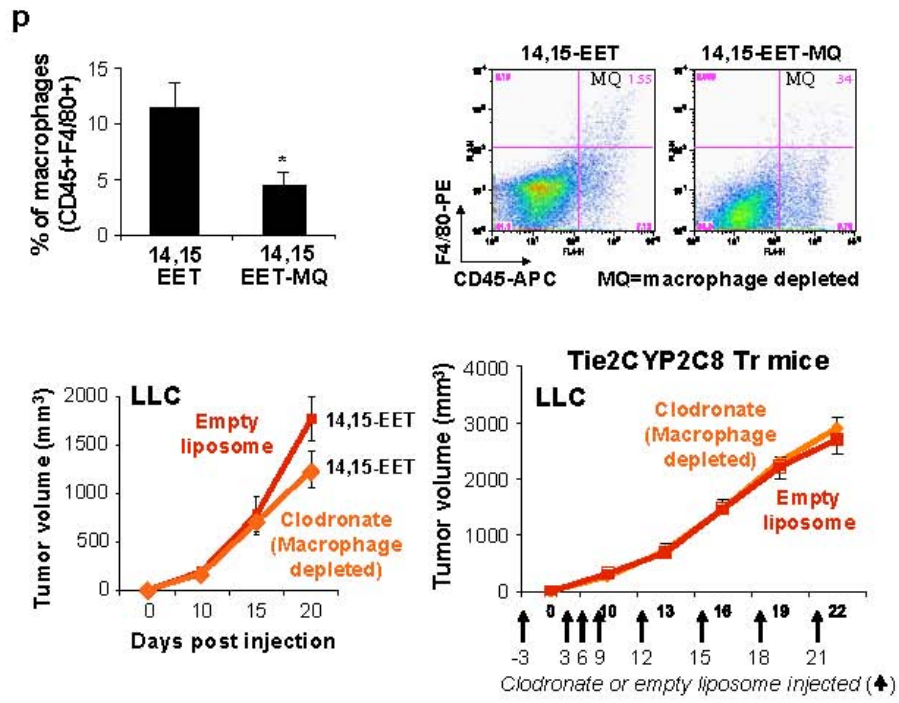
Supplementary Figure 1  
Panigrahy et al.



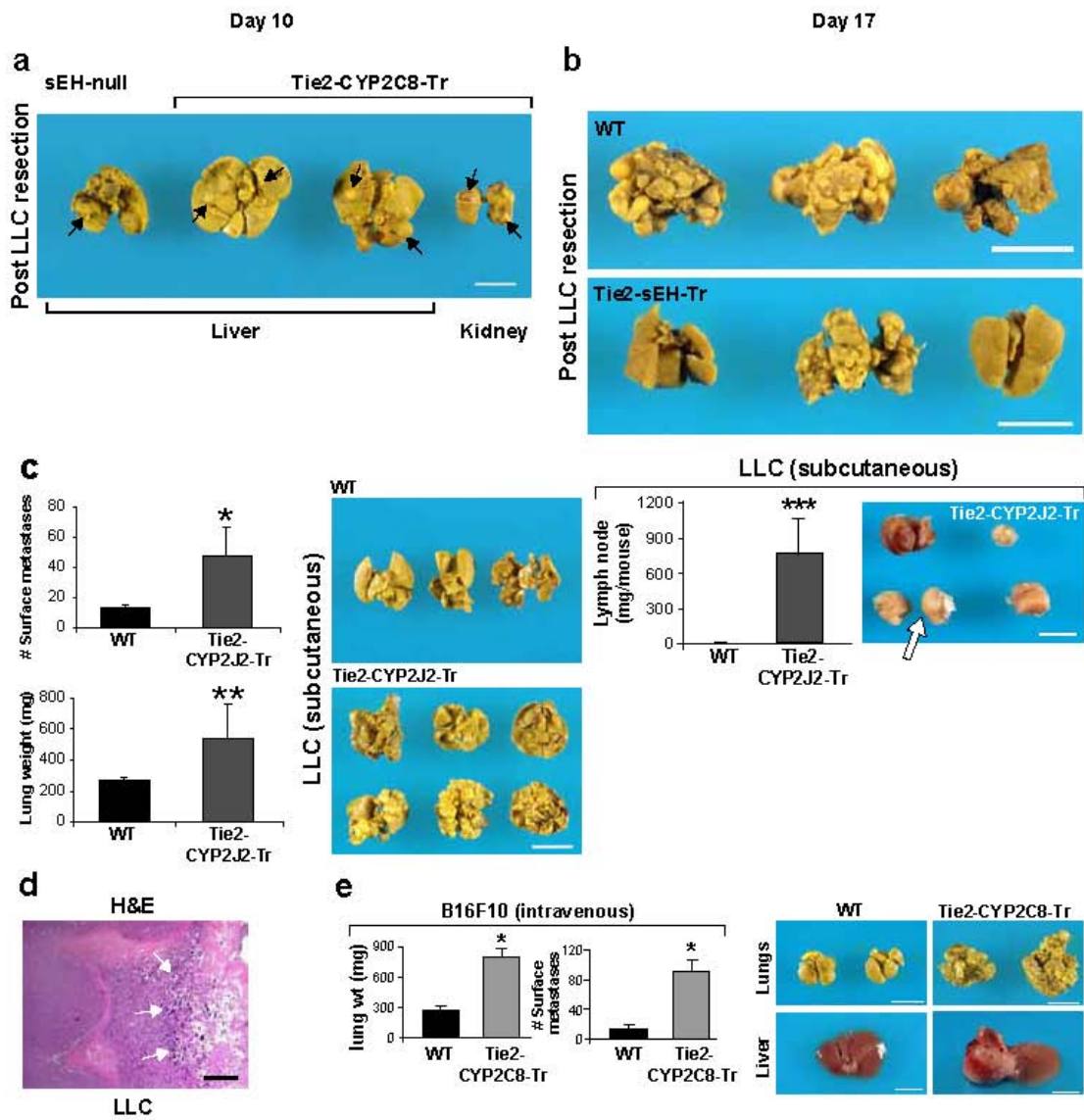
Supplementary Figure 1  
Panigrahy et al.



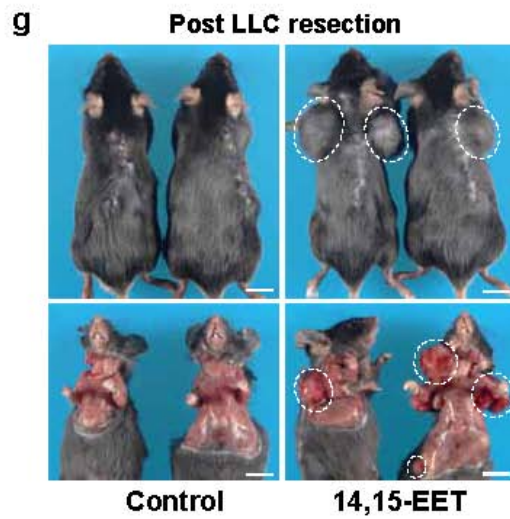
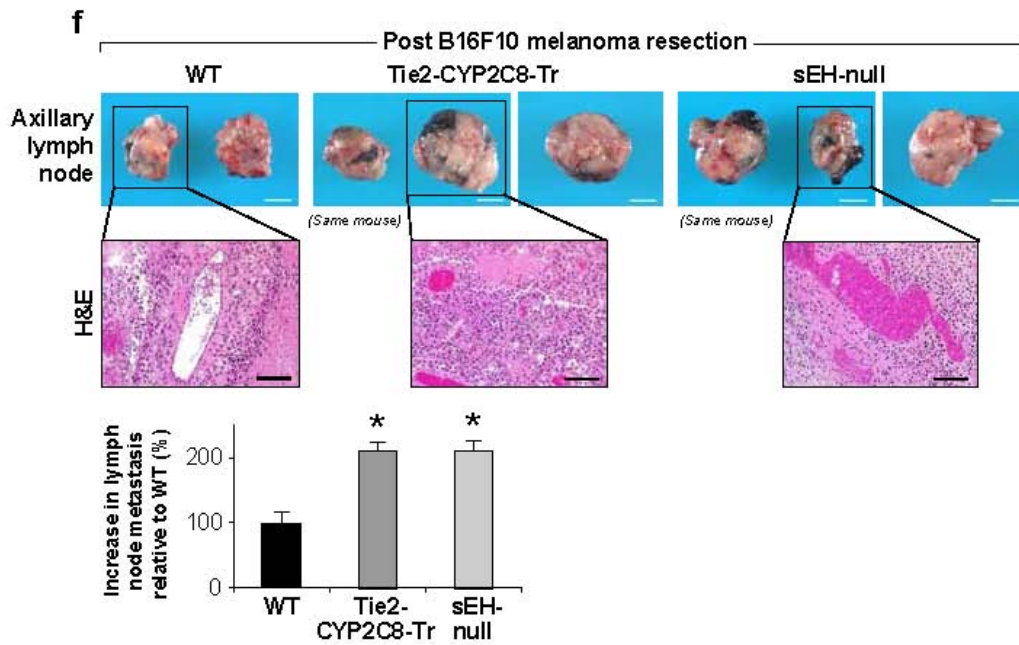
Supplementary Figure 1  
Panigrahy et al.



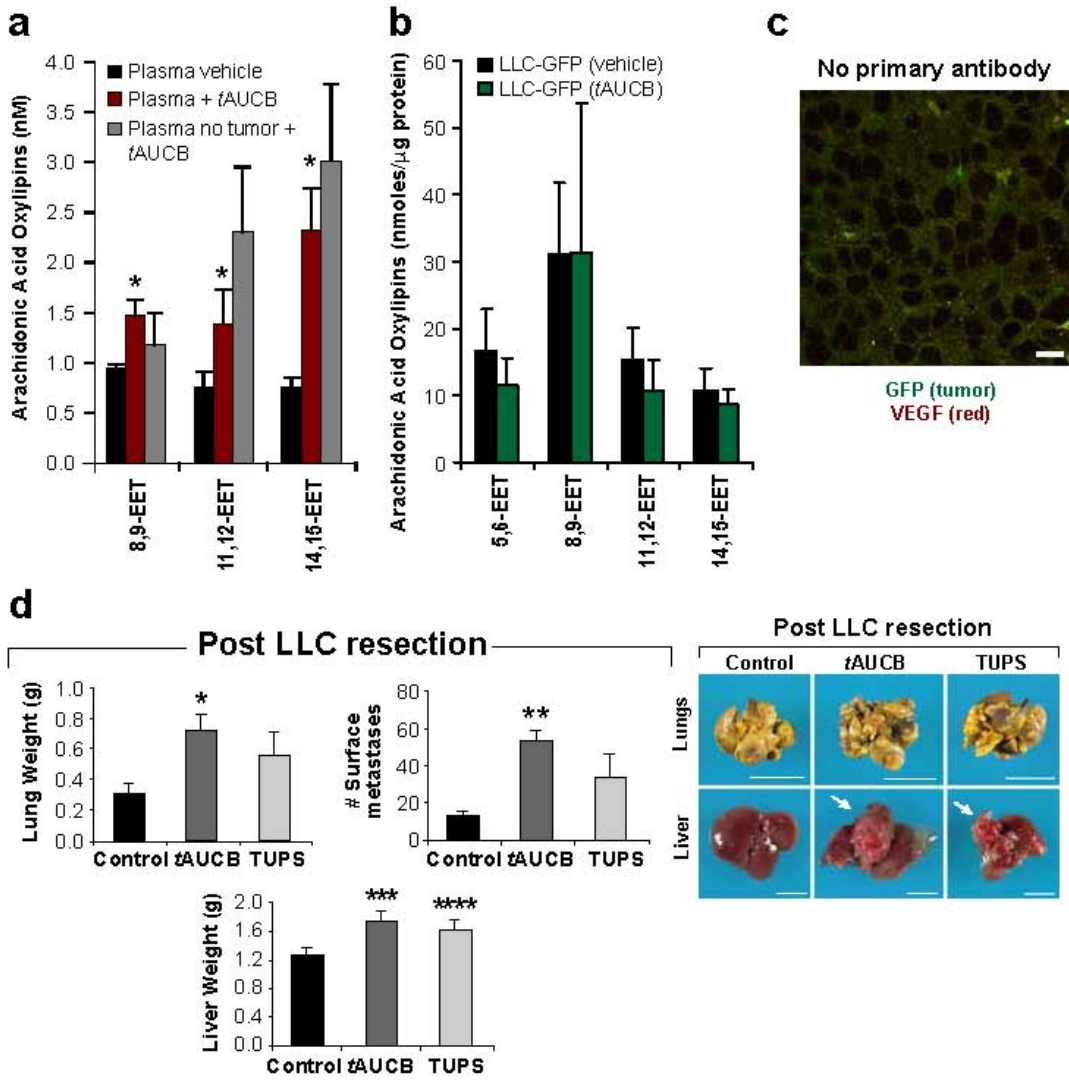
Supplementary Figure 1  
Panigrahy et al.



Supplementary Figure 2  
Panigrahy et al.

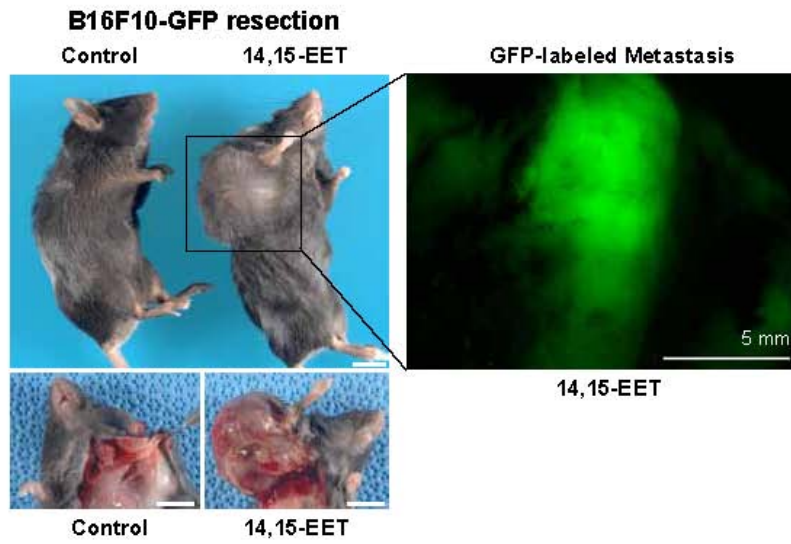


Supplementary Figure 2  
Panigrahy et al.

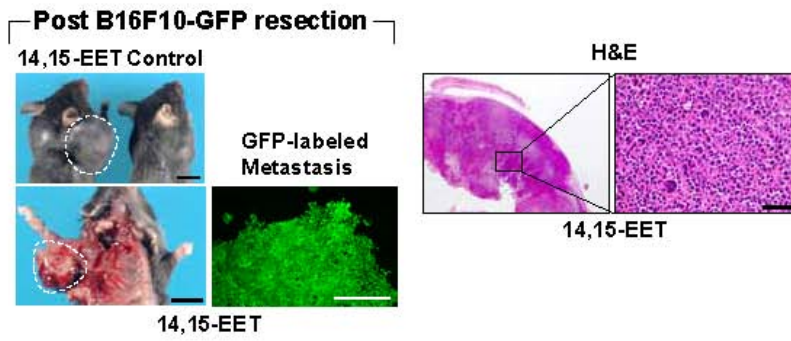


Supplementary Figure 3  
Panigrahy et al.

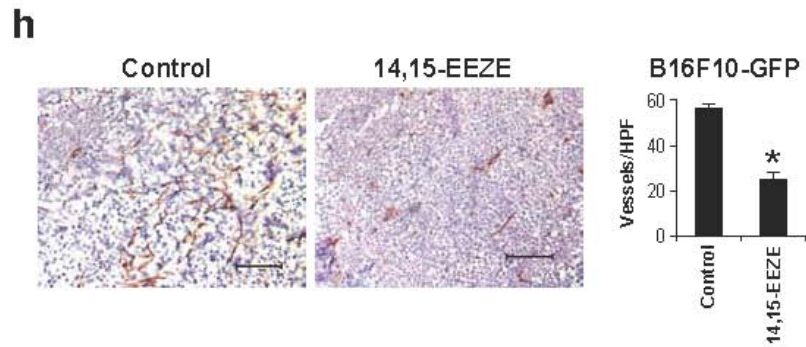
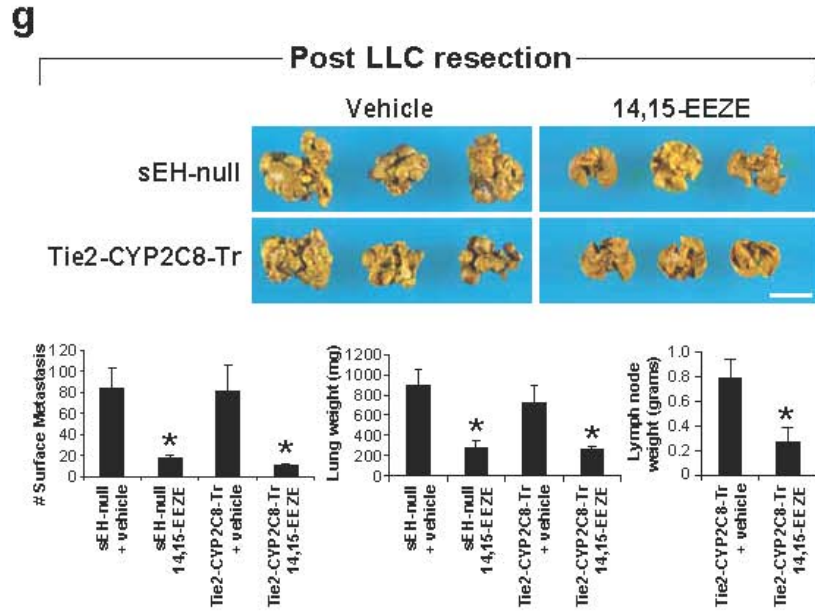
**e**



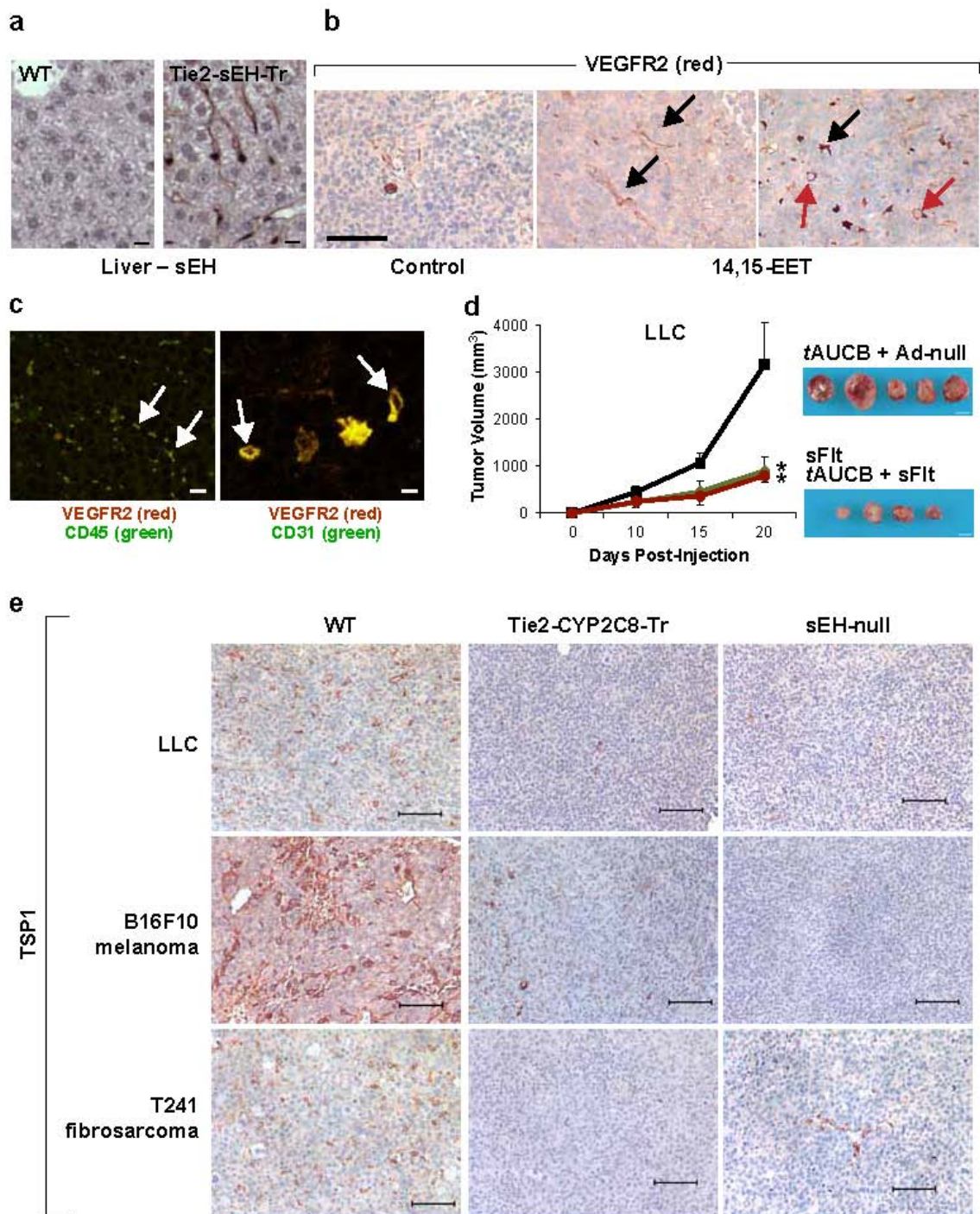
**f**



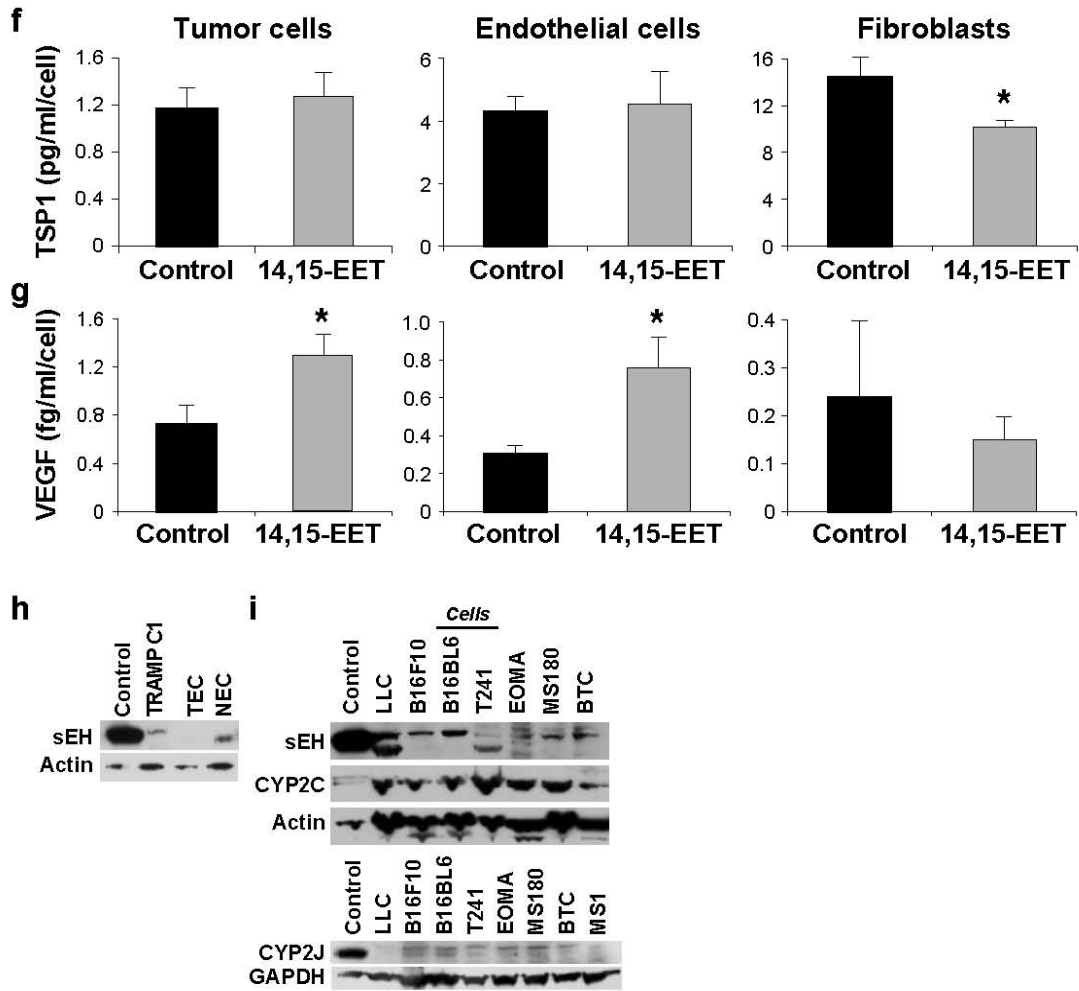
Supplementary Figure 3  
Panigrahy et al.



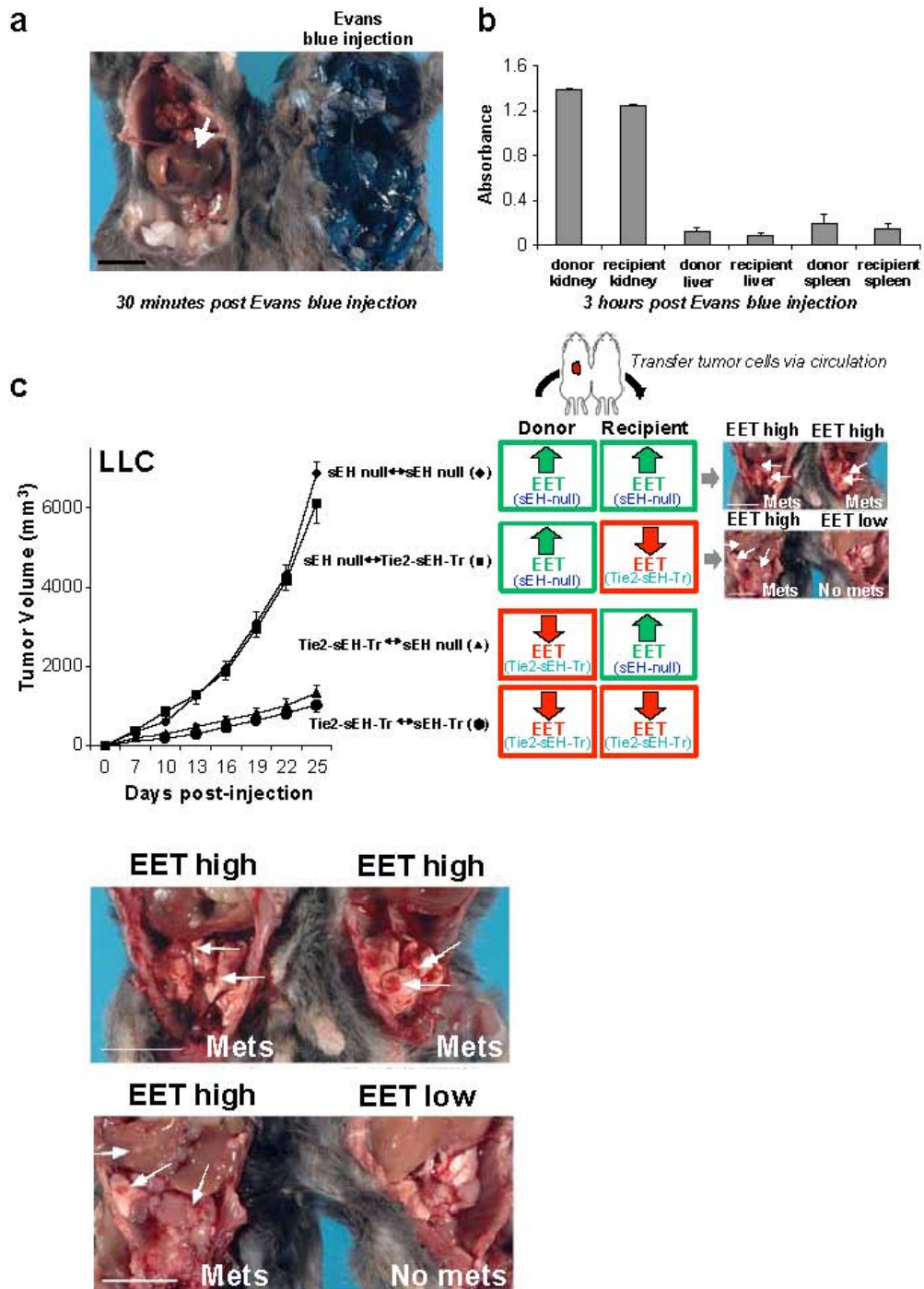
Supplementary Figure 3  
Panigrahy et al.



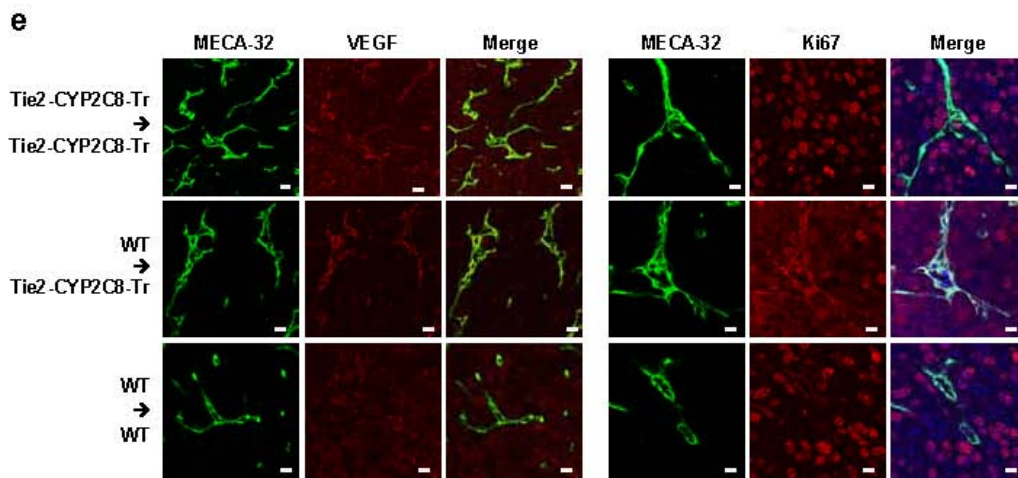
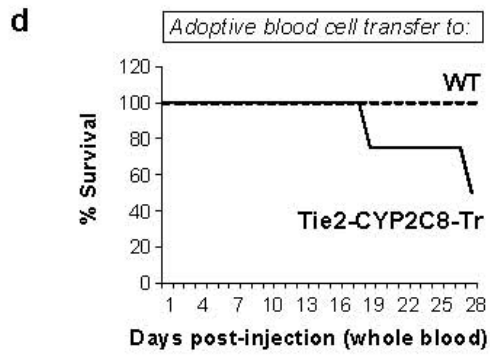
Supplementary Figure 4  
Panigrahy et al.



Supplementary Figure 4  
Panigrahy et al.



Supplementary Figure 5  
Panigrahy et al.



Supplementary Figure 5  
Panigrahy et al.